

Article

Liquid Phase Separation and the Aging Effect on Mechanical and Electrical Properties of Laser Rapidly Solidified $\text{Cu}_{100-x}\text{Cr}_x$ Alloys

Song-Hua Si¹, Hui Zhang^{1,*}, Yi-Zhu He¹, Ming-Xi Li¹ and Sheng Guo²

¹ School of Materials Science and Engineering, Anhui University of Technology, Ma'anshan, Anhui 243002, China; E-Mails: sisonghua@ahut.edu.cn (S.-H.S); heyizhu@ahut.edu.cn (Y.-Z.H.); limingxi@ahut.edu.cn (M.-X.L.)

² Surface and Microstructure Engineering Group, Department of Materials and Manufacturing Technology, Chalmers University of Technology, SE-41296, Gothenburg, Sweden; E-Mail: sheng.guo@chalmers.se

* Author to whom correspondence should be addressed; E-Mail: huizhang@ahut.edu.cn; Tel.: +86-13865606861; Fax: +86-555-2311570.

Academic Editor: Hugo F. Lopez

Received: 18 September 2015 / Accepted: 6 November 2015 / Published: 12 November 2015

Abstract: Duplex structure Cu-Cr alloys are widely used as contact materials. They are generally designed by increasing the Cr content for the hardness improvement, which, however, leads to the unfavorable rapid increase of the electrical resistivity. The solidification behavior of $\text{Cu}_{100-x}\text{Cr}_x$ ($x = 4.2, 25$ and 50 in wt.%) alloys prepared by laser rapid solidification is studied here, and their hardness and electrical conductivity after aging are measured. The results show that the Cu-4.2%Cr alloy has the most desirable combination of hardness and conductive properties after aging in comparison with Cu-25%Cr and Cu-50%Cr alloys. Very importantly, a 50% improvement in hardness is achieved with a simultaneous 70% reduction in electrical resistivity. The reason is mainly attributed to the liquid phase separation occurring in the Cu-4.2%Cr alloy, which introduces a large amount of well-dispersed sub-micron-scale Cr-rich particulates in the Cu-rich matrix.

Keywords: laser cladding; Cu-Cr alloy; liquid phase separation; electrical conductivity

1. Introduction

Great research interest has been devoted to Cu-Cr alloys in the past few decades as the alloys are the most commonly used contact materials in medium-voltage and high-current vacuum interrupters [1–3]. It has been well known that a liquid miscibility gap exists in the Cu-Cr binary phase diagram, due to a large positive mixing heat between Cu and Cr in the liquid state. Once the Cu-Cr melt achieves a sufficient undercooling and cools into the liquid miscibility gap, the Cr-rich strengthening phase will nucleate through the liquid phase separation (LPS) process and form particulates to disperse in the Cu-rich matrix [1–3]. Numerous explorations, mostly by the containerless solidification, have been made to investigate the undercooling effect in Cu-Cr alloys and it has been proved that the properties of Cu-Cr alloys are strongly dependent on their solidification behavior, compositions, aging effects, and also the morphology of the Cr phase [3–5]. In general, the Cr content is designed to range from 25 to 50 wt.% to obtain a good combination of mechanical and electrical properties by optimizing the duplex structure [6,7]. However, the containerless solidification process can only prepare small-sized samples. It is hard to obtain sufficient undercooling in fabricating Cu-Cr alloys with a certain thickness and large contact area for industrial applications. Laser surface cladding seems to be a desirable route to fabricate Cu-Cr alloys if the target is for engineering applications, where a concentrated laser beam is used to fuse a designed alloy coating with a thickness of larger than 1 mm. The laser cladding process has distinctive advantages, such as a rapid solidification rate (10^3 – 10^6 °C/s), forming fine microstructure and a metallurgical bonding interface. Furthermore, the rapid solidification of the laser process can lead to a high undercooling, having a significant effect on non-equilibrium solute trapping and improving the solubility [8,9]. Therefore, it is interesting to study the solidification behavior, microstructure, and mechanical and electrical properties of laser rapidly solidified Cu-Cr alloys, with various Cr contents, which constitutes the topic of the current work.

2. Experimental Section

Various $\text{Cu}_{100-x}\text{Cr}_x$ ($x = 4.2, 25$ and 50 in wt.%) alloy powders were mixed from elemental copper and chromium powders with the purity of 99.9%. The particle size of the elemental powders ranged from 50 to 120 μm . The powder mixture was placed onto the surface of a low-carbon steel (C: 0.17, Mn: 0.08, Si: 0.37, S: 0.039, P: 0.036, Fe: balance in mass percentage) to form a powder bed with a thickness of about 1.8 mm. A 5 kW TJ-HLT5000-type continuous-wave CO_2 -laser system was used for cladding, with about 0.5 L/min high-purity argon supplied through the coaxial nozzle to prevent oxidation. The used laser power was 1.8 kW, the diameter of the laser beam was 4.5 mm, and the laser feed rate was 600 mm/min. The pre-placed powder mixture was melted by moving the laser beam, and a single track alloy with a final thickness of ~ 1.5 mm was formed on the substrate and was cooled in air. To investigate the heat treatment effect, the as-solidified alloy was aged for 50 min at temperatures from 200 to 600 °C.

The microstructures of the as-solidified alloys were observed on a finely polished and etched surface under the scanning electron microscope (SEM, JSM-6490, JEOL, Tokyo, Japan), equipped with the energy dispersive spectrometer (EDS, GENESIS Apex, EDAX, Mahwah, NJ, USA). The

Vickers hardness was measured on the polished surface by applying a load of 4.9 N for 20 s. The electrical resistivity of the as-solidified and aged alloys was measured near the center of the single track alloy using a SZT-2-type four-probe instrument. The low-carbon steel substrate was removed by grinding before the electrical resistivity measurement.

3. Results

3.1. Solidification Behavior and Microstructures

Figure 1a shows an overview of the cross-sectional microstructure of the Cu-4.2%Cr single track alloy. It can be seen that a large amount of spherical white Cr-rich phases are observed and well dispersed in the dark Cu-rich matrix, suggesting that the LPS can occur in the Cu-4.2%Cr alloy. Laser rapid solidification can provoke a large dynamical undercooling and prevent the growth and coalescence of Cr-rich particulates. In this case, the existing time of the laser-melted pool is too short for each droplet to coalesce, and these finely dispersed Cr-rich phases with spherical morphology formed at the early stage during LPS therefore remained in the Cu-rich matrix.

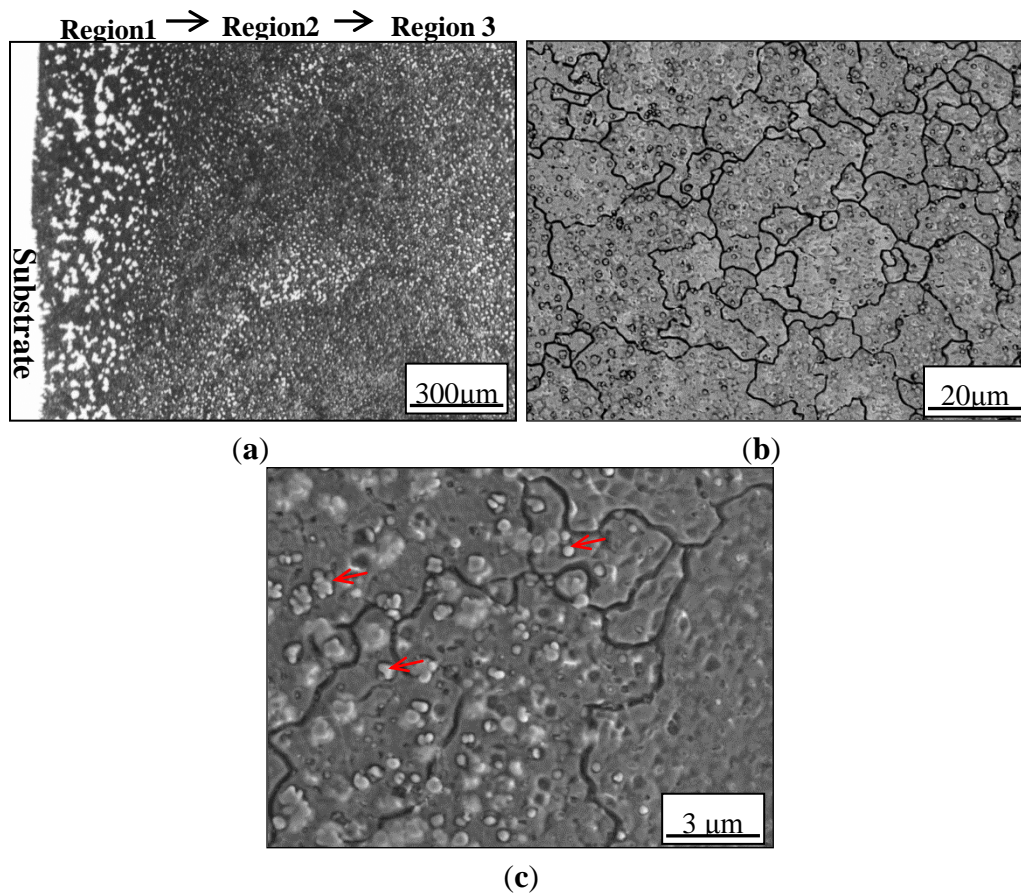


Figure 1. The cross-sectional microstructures in the Cu-4.2%Cr alloy: (a) an overview of the single track alloy; (b) the equiaxed Cu-rich matrix in the center area of alloy; (c) the sub-micron-scale Cr-rich spherical particulates dispersed in the matrix.

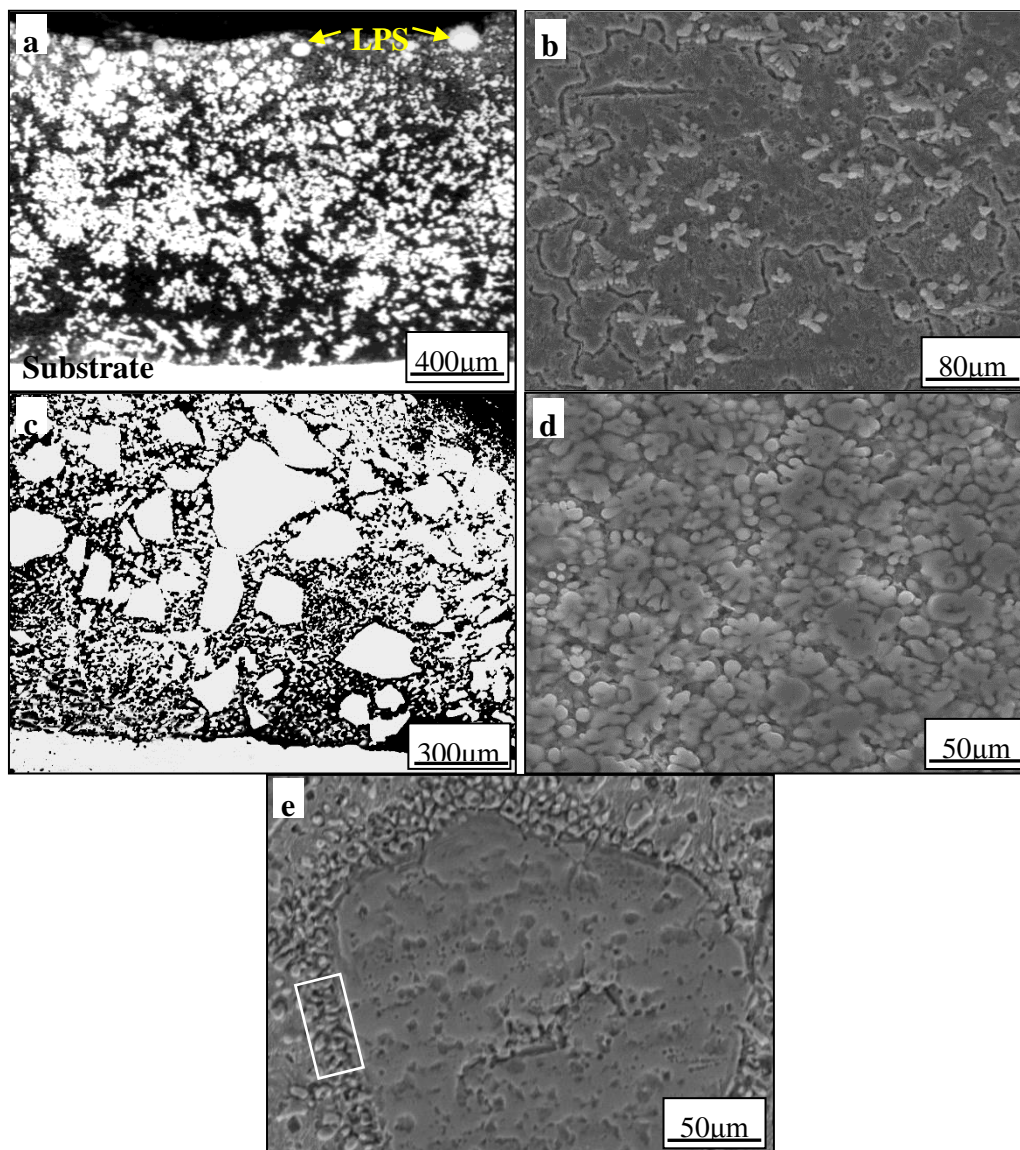


Figure 2. The cross-sectional microstructure in the Cu-25%Cr and Cu-50%Cr alloys: (a) the overall morphology of the Cu-25%Cr alloy; (b) the enlarged dendritic Cr-rich phase dispersed in the center area of the Cu-25%Cr alloy; (c) the overview of the Cu-50%Cr alloy; (d) the Cr-rich phase dispersed in the Cu-50%Cr matrix; (e) the Cr-rich particulate coalesces to about several hundred microns in diameter in the Cu-50%Cr alloy.

Meanwhile, it can be seen that there are three distinctive regions in the cross-sectional microstructure according to the particle size distribution of the Cr-rich phase. Near the substrate (region 1), Cr-rich particles have a larger size of about several tens of microns in diameter. In the central area (region 2) of the alloy, the particle sizes of the Cr-rich phase decrease sharply and have diameters on the sub-micron-scale, as shown in the enlarged microstructure in Figure 1b,c. The Cr-rich phase was labeled by red arrows in Figure 1c. In region 3, near the surface of the alloy, the particle sizes and content of Cr-rich droplets slightly increase again and are a little larger than those in region 2. EDS measurements show that the solubility of Cr in the Cu-rich matrix gradually increases from region 1 to region 3, with the averaged value increase from 2.8, 4.3, to 5.2 wt.%. This increase can be attributed to the lower density and, hence, the floating tendency of the Cr-rich liquid in the

laser-melted pool. According to previous descriptions of the melt and the solidification process in the laser-melted pool, the crystal growth velocity (v) depends on the location and is linked to the heat source velocity (*i.e.*, laser feed rate, v_s) [10,11]. The crystal growth velocity, v , will increase rapidly from zero at the bottom of the alloy to a value close to v_s at the surface, and is accompanied with a decrease of the time interval (Δt) between the start of liquid separation and solidification. Therefore, in region 1, where there is the lowest crystal growth velocity (v) and the longest time interval (Δt), the Cr-rich liquid phase will coalesce and have a large particle size. In region 2, Δt decreases greatly with the rapid increase of the v , where the sub-micron-scale Cr-rich liquid phase formed during LPS has no sufficient time to coalesce and maintains a very fine particle size. In region 3, where there is the highest solute content of Cr, the chance of the coalescence for the increased amount of Cr-rich liquid phase droplets increases, resulting in the slight increase of particle size and content of the Cr-rich phase compared to that in the center of the alloy.

Figure 2a,b show the overview and typical dendritic microstructures of the Cr-rich phase in the Cu-25%Cr alloy, respectively. The feature size of the Cr-rich phase is approximate 50 μm and it grows into the dendritic morphology, indicating that the well-distributed Cr-rich phase is not formed via LPS, possibly due to the insufficient undercooling. Meanwhile, some spherical Cr-rich particulates appear near the surface of the alloy, as marked in Figure 2a, indicating that LPS can occur in some local areas of the alloy, where there is sufficient solidification rate and undercooling. Figure 2c shows the overview of the Cu-50%Cr alloy; the high Cr content in the Cu-50%Cr composition leads to the unavoidable coalescence of Cr-rich particulates. As a consequence, many large-sized Cr-rich phases about several hundreds of microns in diameter are formed. Figure 2d shows the nearly spherical morphology of Cr-rich particulates in the matrix of Cu-50%Cr alloy. In the Figure 2e it can be seen that the spherical structure of Cr-rich phases extends with some protrusions (marked by the square) around the edges of large-sized Cr-rich particles, suggesting that separated melts reject solutes during solidification, and some interaction occurs at the interface of neighboring melts.

3.2. The Effect of Aging

The hardness measurement is conducted on the cross-section of the single track alloy and measured five times. Figure 3 shows the mean hardness distribution in the Cu-Cr alloys directly after laser rapid solidification. For the Cu-50%Cr alloy, the hardness distribution is not very even, mainly due to the large size of the Cr-rich phase. For Cu-25%Cr and Cu-4.2%Cr alloys, the hardness increases from the bottom to the surface due to the increased solutioning of Cr. Figure 4a shows the average hardness in the Cu-Cr alloys after the aging treatment, while Figure 4b presents the electrical resistivity revolution of the alloys, which were measured by a four-probe instrument and only one time. Interestingly, the Cu-4.2%Cr alloy has the highest hardening effect, and the hardness increases from 116 HV in the as-solidified state to 172 HV after aging at 500 °C, while at the same time the electrical resistivity decreases from 10.1 to 3.2 $\mu\Omega\cdot\text{cm}$. As for the Cu-25%Cr and Cu-50%Cr alloys, the hardness increases slowly from 186 to 202 HV and from 203 to 219 HV, respectively, while the electrical resistivity decreases from 22.1 to 10.4 $\mu\Omega\cdot\text{cm}$ and from 26.9 to 13.9 $\mu\Omega\cdot\text{cm}$, respectively. Considering its lowest electrical resistivity while still having a hardness comparable to that of Cu-25%Cr and Cu-50%Cr, the

laser rapidly solidified Cu-4.2%Cr alloy is considered to have the most desirable combination of hardness and electrical conductivity, and noticeably this is achieved at a very low Cr content.

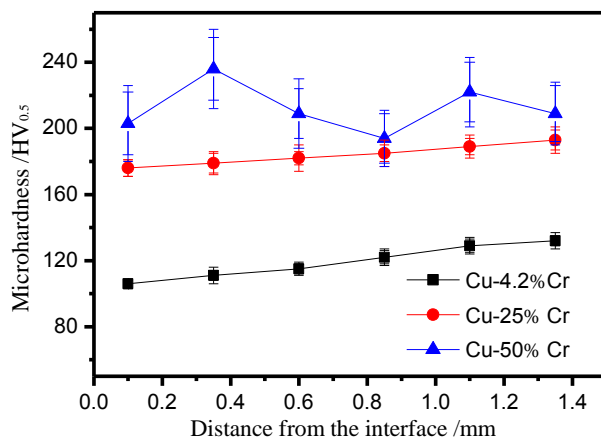


Figure 3. Cross-sectional hardness distribution in the Cu-Cr alloys.

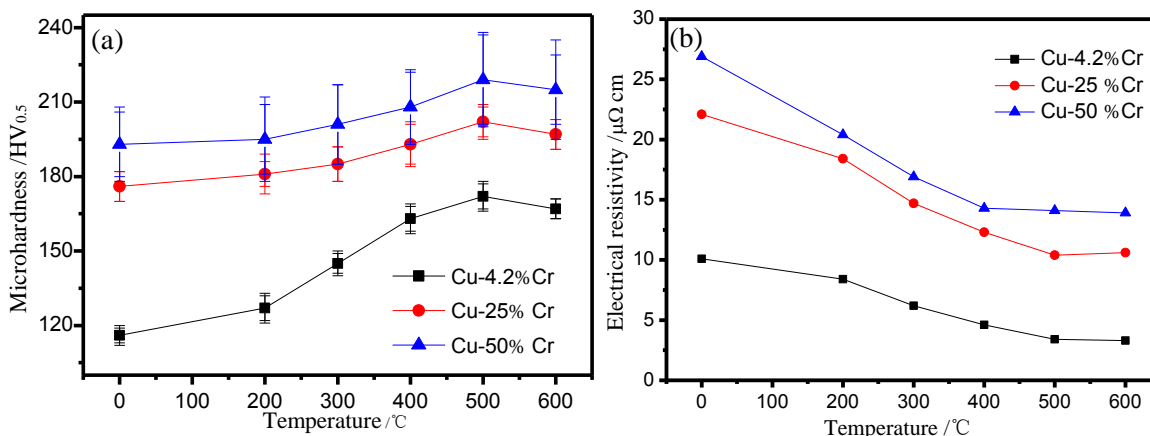


Figure 4. Evolution of properties after aging in the Cu-Cr alloys: (a) hardness; (b) electrical resistivity.

4. Discussion

There are two phase diagrams of the Cu-Cr alloy system according to previous research [12,13]. Muller *et al.* gave the equilibrium phase diagram of the Cu-Cr alloy system, and considered that it is monotectic with a stable liquid miscibility gap between 40 to 94.5 wt.% Cr. Recently, it has been argued that the Cu-Cr system has a metastable liquid miscibility gap from thermodynamic calculations, as replotted in Figure 5 [13]. Before we conducted experiments, the composition of the Cu-Cr alloy was designed according to Muller's equilibrium phase diagram and set to be Cu-50%Cr (in the miscibility gap), Cu-25%Cr (in the middle of the hypereutectic zone), and Cu-4.2%Cr (very close to the eutectic composition). However, our experiment results here show that LPS can occur in the Cu-4.2%Cr, Cu-50%Cr, and at the surface of Cu-25%Cr alloys, providing support for the existence of a metastable liquid miscibility gap in Figure 5. When the Cu-Cr alloy is undercooled below some temperature depending on the composition, the liquid phase will separate into two liquids. According to Figure 5, the undercooling for Cu-25%Cr (23.4 at.% Cr) is smaller than that in Cu-4.2%Cr (5.1 at.%

Cr) and Cu-50%Cr (55 at.% Cr). Therefore, it could be difficult for LPS to occur in the Cu-25%Cr (23.4 at.% Cr) alloy, and the Cr-rich phase grows into the dendritic morphology. As for the Cu-50%Cr (55.0 at.% Cr) alloy, although LPS still occurs, it is difficult to avoid the coalescence of the Cr-rich particulates due to the high Cr content. In the Cu-4.2%Cr (5.1 at.% Cr) alloy, it is seen that sub-micron-scale Cr-rich spherical particulates are well dispersed in the Cu-rich matrix, due to the laser rapid solidification process which supplies a sufficient undercooling and introduces LPS. The aging treatment at 500 °C leads to a ~50% improvement in hardness and a 70% reduction in electrical resistivity. The reduced electrical resistivity can be attributed to the weakened electron scattering effect after aging, while the hardness increase is due to the precipitation hardening. To understand the relationship between aging properties and microstructure evolution, further investigations conducted by TEM should be done.

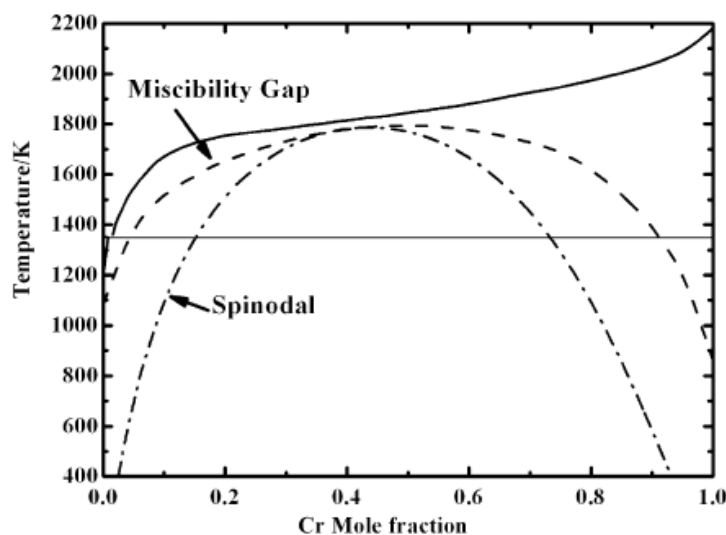


Figure 5. Cu-Cr binary phase diagram with metastable liquid miscibility gap predicted by thermodynamic calculations, replotted after Ref. [13].

5. Conclusions

To summarize, a duplex structure with well-dispersed sub-micron-scale Cr-rich particulates via the LPS process has been successfully achieved in the laser rapidly solidified Cu-4.2%Cr alloy. In the Cu-50%Cr alloy, Cr-rich particulates formed during LPS are easily coalesced with a particle size of about several hundreds of microns, leading to an uneven hardness distribution. No LPS is observed in the Cu-25%Cr alloy due to the insufficient undercooling. Aging at 500 °C leads to a 50% improvement in hardness (from 116 to 172 HV) and, simultaneously, a 70% reduction in electrical resistivity (from 10.1 $\mu\Omega\cdot\text{cm}$ to 3.2 $\mu\Omega\cdot\text{cm}$) in the Cu-4.2%Cr alloy, giving the most desirable combination of hardness and electrical conductivity.

Acknowledgments

The authors thank the financial support from the National Natural Science Foundation of China under Grants No. 51271001 and No. 51445005, the University Natural Science Research Project of

Anhui Province of China under Grant No. KJ2014A029, and the Tribology Science Fund of State Key Laboratory of Tribology under Grant No. SKLTKF14B02.

Author Contributions

Song-Hua Si, Hui Zhang and Sheng Guo wrote the paper and contributed to all the activities related to this paper. Yi-Zhu He and Ming-Xi Li contributed to the discussion.

Conflicts of Interest

The authors declare no conflict of interest.

References

1. Bachmaie, A.; Rathmayr, G.B.; Bartosik, M.; Apel, D.; Zhang, Z.; Pippan, R. New insights on the formation of supersaturated solid solutions in the Cu-Cr system deformed by high-pressure torsion. *Acta Mater.* **2014**, *69*, 301–313.
2. Fu, Y.B.; Cui, J. Preparation of Cu-Cr-Zr alloy billets by horizontal electromagnetic continuous stirring. *Sci. Technol.* **2014**, *30*, 370–376.
3. Lin, G.B.; Wang, Z.D.; Zhang, M.K.; Zhang, H.; Zhao, M. Heat treatment method for making high strength and conductivity Cu–Cr–Zr alloy. *Mater. Sci. Technol.* **2011**, *27*, 966–969.
4. Zhou, Z.M.; Wang, Y.P.; Gao, J.; Kolbe, M. Microstructure of rapidly solidified Cu-25 wt.% Cr alloys. *Mater. Sci. Eng. A* **2005**, *398*, 318–322.
5. Gao, J.; Wang, Y.P.; Zhou, Z.M.; Kolbe, M. Phase separation in undercooled Cu-Cr melts. *Mater. Sci. Eng. A* **2007**, *449–451*, 654–657.
6. He, W.X.; Yu, Y.; Wang, E.D.; Sun, H.F.; Hu, L.X.; Chen, H. Analysis of phase in Cu-15%Cr-0.24%Zr alloy. *Trans. Nonferrous Met. Soc. China* **2013**, *23*, 1342–1348.
7. Zhao, Q.; Shao, Z.B.; Liu, C.J.; Jiang, M.F.; Li, X.T.; Zevenhoven, R.; Saxen, H. Preparation of Cu-Cr alloy powder by mechanical alloying. *J. Alloy. Compd.* **2014**, *607*, 118–124.
8. Pan, M.; Konda, G.; Prashanth, S.S.; Jia, Y.D.; Wang, H.W.; Zou, C.M.; Wei, Z.J.; Jürgen, E. Influence of Annealing on Mechanical Properties of Al-20Si Processed by Selective Laser melting. *Metals* **2014**, *4*, 28–36.
9. Zhang, H.; He, Y.Z.; Pan, Y. Enhanced hardness and fracture toughness of the laser-solidified FeCoNiCrCuTiMoAlSiB_{0.5} high-entropy alloy by martensite strengthening. *Scr. Mater.* **2013**, *69*, 342–345.
10. Holger, S.; Konda, G.P.; Lukas, L.; Uta, K.; Jürgen, E.; Poprawe, R. Selective Laser Melting of Ti-45Nb Alloy. *Metals* **2015**, *5*, 686–694.
11. Yue, T.M.; Xie, H.; Lin, X.; Yang, H.O.; Meng, G.H. Microstructure of Laser Re-Melted AlCoCrCuFeNi High Entropy Alloy Coatings Produced by Plasma Spraying. *Entropy* **2013**, *15*, 2833–2845.
12. Muller, R. Arc-melted Cu-Cr alloys as contact materials for vacuum interrupters. *SiemensForsch—UEntwick—Ber Bd.* **1988**, *17*, 105–115.

13. Wei, X.; Wang, J.P.; Yang, Z.M.; Sun, Z.B.; Yu, D.M.; Song, X.P.; Ding, B.J.; Yang, S. Liquid phase separation of Cu–Cr alloys during the vacuum breakdown. *J. Alloy. Compd.* **2011**, *509*, 7116–7120.

© 2015 by the authors; licensee MDPI, Basel, Switzerland. This article is an open access article distributed under the terms and conditions of the Creative Commons Attribution license (<http://creativecommons.org/licenses/by/4.0/>).